Science Translational Medicine
AAAS

stm.sciencemag.org/cgi/content/full/12/527/eaax1501/DC1

Supplementary Materials for

The IDH-TAU-EGFR triad defines the neovascular landscape of diffuse gliomas

Ricardo Gargini, Berta Segura-Collar, Beatriz Herránz, Vega García-Escudero, Andrés Romero-Bravo, Felipe J. Núñez, Daniel García-Pérez, Jacqueline Gutiérrez-Guamán, Angel Ayuso-Sacido, Joan Seoane, Angel Pérez-Núñez, Juan M. Sepúlveda-Sánchez, Aurelio Hernández-Laín, María G. Castro, Ramón García-Escudero, Jesús Ávila*, Pilar Sánchez-Gómez*

*Corresponding author. Email: psanchez@isciii.es (P.S.-G.); jesus.avila@csic.es (J.A.)

Published 22 January 2020, *Sci. Transl. Med.* **12**, eaax1501 (2020)
DOI: 10.1126/scitranslmed.aax1501

The PDF file includes:

Other Supplementary Material for this manuscript includes the following:

(available at stm.sciencemag.org/cgi/content/full/12/527/eaax1501/DC1)

Supplementary Material

Materials and Methods

DNA constructs and lentiviral/retroviral production

The lentivirus that encodes the longest wild type isoform of Tau in human brain harboring four repeats and two N-terminal inserts followed by GFP linked by an IRES was a gift from by Prof. Kenneth S. Kosik (UC Santa Barbara). As a control we used a lentivector encoding E-GFP, pRRLSIN.cPPT.PGK-GFP.WPRE (Addgene plasmid 12252). pLV-Hygro-Luciferase (VectorBuilder #VB150916-10098) was used as reporter. Lentiviral vector to express shRNAs were: shCD248 (Sigma #SHCLNG-NM_020404: TRCN0000053455, TRCN0000053457, TRCN00000443679, TRCN00000429396, TRCN0000043782) and shTAZ (TRCN0000370006, TRCN0000370007). Retroviral vectors used were pBabe-EGFR wt (#11011), MSCV-XZ066-GFP-EGFR vIII (#20737), pBabe-puro-Flag-IDH1 (#62923), pBabe-puro-Flag-IDH1-R132H (#62924) (Addgene) and pBabePuroTAZ-WT was a generous gift from Kun-Liang Guan. To obtain the virus, the 293T cells were transiently co-transfected with 5 μg of appropriate lentivector plasmid, 5 μg packaging plasmid pCMVdR8.74 (Addgene #Plasmid 22036) and 2 μg VSV-G envelope protein plasmid pMD2G (Addgene #Plasmid 12259) using Lipofectamine Plus reagent (Invitrogen). Retrovirus and lentivirus supernatant was prepared by transfection of 293T cells and collection of the supernatant 48 hr after.

Growth curve and sphere formation assay

Glioma cells were infected by the control lentivirus (LV-GFP) or lentivirus directing expression of TAU (LV-TAU-GFP). The tumor spheres were Accumax-dissociated to single cells, and 500/1000 cells of each condition were plated in a p24-well-plate in triplicate. Five days after plating, spheres and cell number were measured.

EGFR degradation experiment

GFP or TAU SVZ EGFRwt/amp cells were grown in stavirng media for 1h and then EGF (100 ng/ml) was added and the cells were incubated in the presence of DMSO, MG132 or Chloroquine for 2h. Then, cells were collected and lysed and subsequently analyzed by western blot, as described below.

Endothelial cell sprouting assay

In order to generate endothelial cell spheroids, $1x10^6$ cells of HMBEC were suspended in CM and seeded in nonadherent plates. These spheroids were harvest within 48 hours and embedded into matrigel in 96-well plates with conditioned medium generated for each cell line. After 24 h, sprouting was induced and the number of sprouts for each spheorid were quantified. For the generation of the conditioned media, RG1 (GFP or Tau) were grown during 48 hours in serum-free culture media (DMEM-F12 supplemented with FGF2 (50ng/ml) and penicillin-streptomycin). The medium was filtered with a 70-μm filter before use.

Intracranial tumor formation and treatment in vivo

Animal experiments were reviewed and approved by the Research Ethics and Animal Welfare Committee at "Instituto de Salud Carlos III" (PROEX 244/14 and 02/16), in agreement with the European Union and national directives. Intracranial transplantation to establish orthotopic xeno- and allo-grafts was performed injecting 100.000-300.000 cells (resuspended in 2 μl of culture stem cell medium) with a Hamilton syringe into athymic Nude-Foxn1nu brains (Harlan Iberica). The injections were made into the striatum (coordinates: A–P, −0.5 mm; M–L, +2 mm, D–V, −3 mm; related to Bregma) using a Stoelting Stereotaxic device. When applicable, tumor growth was monitored in an IVIS equipment (Perkin Elmer) after intraperitoneal injection of D-luciferin (75 mg/Kg) (PerkinElmer). The animals were sacrificed at the onset of symptoms. Mice were treated with Epothilone D (Abcam, ab143616) (1 mg/kg two days per week through intra-peritoneal injection) and/or Temozolomide (Sigma Aldrich) (5mg/kg daily through intraperitoneal injection). Epothilone D was dissolved in 4% DMSO +10%Polysorbate. Temozolomide was dissolved in 1% BSA+PBS. Control animals were treated with these solvents.

In vivo limiting dilution assay

Increasin numbers of RG1 (GFP or TAU) cells were re-suspended in CM and Matrigel (BD) (1:10) and injected subcutaneously injected in nude mice. Animals were sacrificed before tumors reached a 1.5 cm in diameter. The statistical significances were calculated using the Extreme Limiting Dilution Analysis software (http://bioinf.wehi.edu.au/software/limdil/ index.html).

Inmunofluorescent (IF) and Inmunohistochemical (IHC) staining

Slides were heated at 60ºC for 1 hour followed by deparaffinization and hydration, washed with water, placed into antigen retrieval solution (pressure cooking) in 10 mM sodium citrate pH 6.0. Paraffin sections were permeabilized with 1% Triton X-100 (Sigma-Aldrich) in PBS and blocked for 1 hour in PBS with 5% BSA (Sigma), 10% FBS (Sigma) and 0,1% Triton X-100 (Sigma). The following primary antibodies (Table S4) were incubated O/N at 4ºC. The second day, sections were washed with PBS three times prior to incubation with the appropriate secondary antibody (Table S4) (1:200 dilution) for 2h at room temperature. Prior to coverslip application, nuclei were counterstained with DAPI and imaging was done with Leica SP-5 confocal microscope. Otherwise, IHC sections were incubated with biotinylated secondary antibodies (1:200 dilution). Target proteins were detected with the ABC Kit and the DAB kit (Vector Laboratories).

IF and IHC quantification

Density measurements of IgG extravasation and Ang2 expression were performed with ImageJ software. The signal from the endomucin channel was subtracted from the IgG or the Ang2 channels. The IHC score was judged from 0 (no staining) to 3 (Tau staining) or 4 (CD248 staining) on those samples with the strongest positive staining. For the longitudinal analysis of the primary and relapsed tumors we calculated the score of 10 high magnification pictures of each sample. The data depicted in Figure 2 E and F is the average of these 10 pictures. For the quantification of the vasculature, we counted the number of dilated vessels per high-magnification field.

Western Blot analysis

Protein content was quantified using BCA Protein Assay Kit (Thermo-Fisher-Scientific). Approximately 20 µg of proteins were resolved by 10% or 12% SDS-PAGE and they were then transferred to a nitro cellulose membrane (Hybond-ECL, Amersham Biosciences). The membranes were blocked for 1 h at room temperature in TBS-T (10 mM Tris-HCl [pH 7.5], 100 mM NaCl, and 0.1% Tween-20) with 5% skimmed milk, and then incubated overnight at 4ºC with the corresponding primary antibody diluted in TBS-T. The primary antibodies and the dilutions are shown in Table S4. After washing 3 times with TBS-T, the membranes were incubated for 2 h at room temperature with their corresponding secondary antibody (HRP-conjugated anti mouse or anti rabbit, DAKO) diluted in TBS-T. Proteins were visible by enhanced chemiluminiscence with ECL (Pierce) using the Amersham Imager 680.

qRT-PCR assay

RNA was extracted from the tissue using RNA isolation Kit (Roche). Total RNA (1µg) was reverse transcribed with PrimeScript RT Reagent Kit (Takara). Quantitative real-time PCR was performed using the Light Cycler 1.5 (Roche) with the SYBR Premix Ex Taq (Takara). The primers used for each reaction are indicated in Table S5. Gene expression was quantified by the delta-delta Ct method.

EGFR Sequencing of primary GBMs

To identify point EGFR mutations, cDNAs from the different cell lines were sequenced using the primers indicated in Table S6. The sequences were aligned and collated with the EGFR transcript (NM_005228.4) in the NIH GenBank database using the multiple sequence alignment tool Clustal Omega (www.ebi.ac.uk/Tools/msa/clustalo/) and the Sequencing Analysis Software v5.3.1 from Applied Biosystems. The identified mutations were analyzed at cBioPortal (www.cbioportal.org).

Gene expression and survival analyses

Tau (MAPT) gene expression and follow-up overall survival data from human glioma tumors corresponding to TCGA Glioblastoma (GBM) and Brain lower grade Glioma (LGG) data sets were downloaded respectively from cBioPortal (http://www.cbioportal.org/) and TCGA databases (http://tcga-data.nci.nhi.gov/docs/publications/lgggbm_2015) using UCSC cancer browser. Kaplan-Meier survival curves were done within TCGA-GBM, TCGA-LGG, TCGA-GBM-LGG, Rembrandt, Gravendeel, Ducray, Freije and Nutt cohorts upon stratification based into low and high groups using expression values from *Tau (MAPT)* gene. Significance of differences in survival between groups was calculated using the log-rank test. These data were obtained from UCSC Xena-Browser (https://xenabrowser.net) and Gliovis (http://gliovis.bioinfo.cnio.es). Classification into classical, mesenchymal, neural and proneural subtypes was retrieved from the TCGA GBM data set (https://www.ncbi.nlm.nih.gov/pubmed/24120142) together with Tau/MAPT expression values. Differences in Tau expression between mesenchymal and other groups were calculated using Student's t-test. In David gene onotology analysis we have used a cluster of 1000 genes co-expressed with Tau/MAPT. They were chosen using the highest values of the Spearman´s correlations. Correlation between gene expression values of MAPT versus other genes was done using Pearson analysis. Gene Set Enrichment Analysis (GSEA) was computed into the TCGA-GBMLGG cohort (RNAseq (IlluminaHiSeq)) using Tau gene expression as a continuous class label and genesets

from the “CGP: chemical and genetic perturbations” and “CP:BIOCARTA: BioCarta gene sets” (n=) from the MSigDB genesets database.

Analysis of methylation of the MAPT gene and CTCF Chip-seq binding

DNA-methylation analysis in human glioma within the MAPT locus was done using the TCGA data (Illumina Infinium HumanMethylation450 platform). Methylation beta values from 56 probes within MAPT locus were retrieved from the Xena browser (https://xenabrowser.net/) together with MAPT gene expression values. Pearson correlation values between each methylation probe and gene expression values, calculated for all samples, was calculated and represented together with the CpG islands located at the MAPT locus (CpG302, CpG26 and CpG21). Both TCGA LGG-GBM and LGG cohorts were individually analyzed. Correlation values were independently calculated for IDH1 mutant or wild-type samples in the TCGA LGG cohort. ChIP-seq analysis using anti-CTCF antibody was performed from profiling in IDH1 mutant and wild-type glioma patient specimens and culture models (GSE70991). Briefly tdf files from GEO repository from both IDH1 mutant and wild-type samples were downloaded and visualized using IGV browser. CTCF occupancy at the CpG islands located from MAPT loci was visualized.

Supplementary Figures

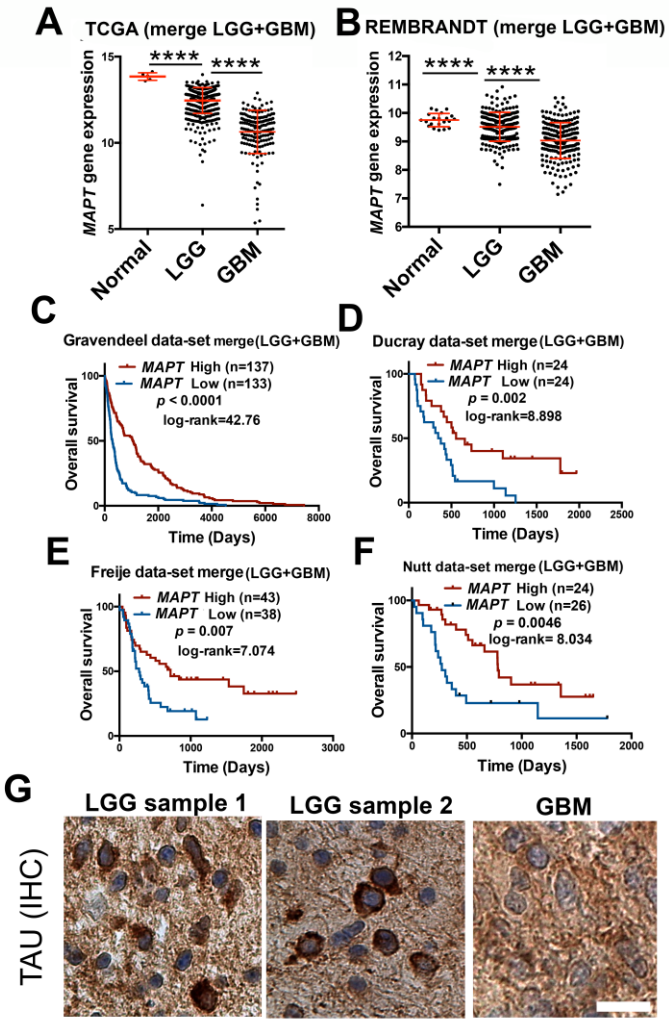

Fig. S1. Association of TAU with the clinical pathology of diffuse gliomas. (**A** and **B**) Analysis of *MAPT* expression by RNAseq in diffuse glioma patients compared to normal tissue, using the TCGA (n=692) (A) and the Rembrandt (n=432) (B) cohorts. Tumors were grouped according to the WHO classification (histological type). (**C-F**) Kaplan-Meier overall survival curves of patients from the Gravendeel (n=276) (**C**); the Ducray (n=48) (**D**); the Freije (n=81) (**E**) and the Nutt (n=60) (**F**) cohorts. Patients in each cohort were stratified into 2 groups based on high and low *MAPT* expression values, log-rank (Mantel-Cox) test. (**G**) Representative pictures of the TAU IHC staining of several gliomas. Data shown as mean ± SD; Student's t test; ****, $p \leq 0.0001$. Scale bar 20 μm.

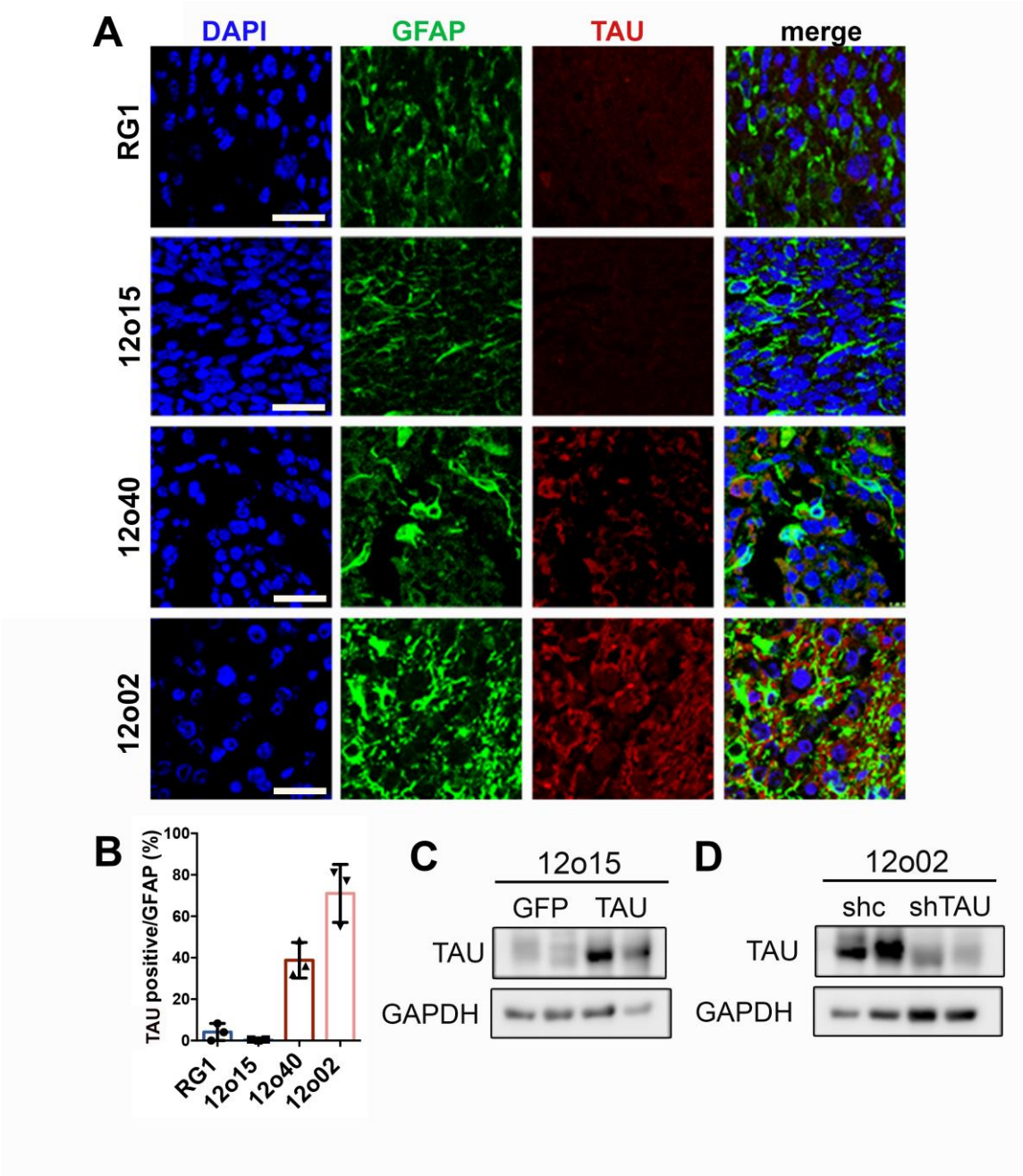

Fig. S2. Expression of TAU in PDX. (**A**) Representative images of TAU and GFAP IF co-staining of tumors from Fig. 2H. (**B**) Quantification of the co-staining of TAU and GFAP in A. (**C-D**) WB analysis and quantification of TAU in the tumors from Fig. 2J (C) and Fig. 2K (D). GAPDH levels were used for normalization. Data shown as mean ± SD. Scale bar 50 μm.

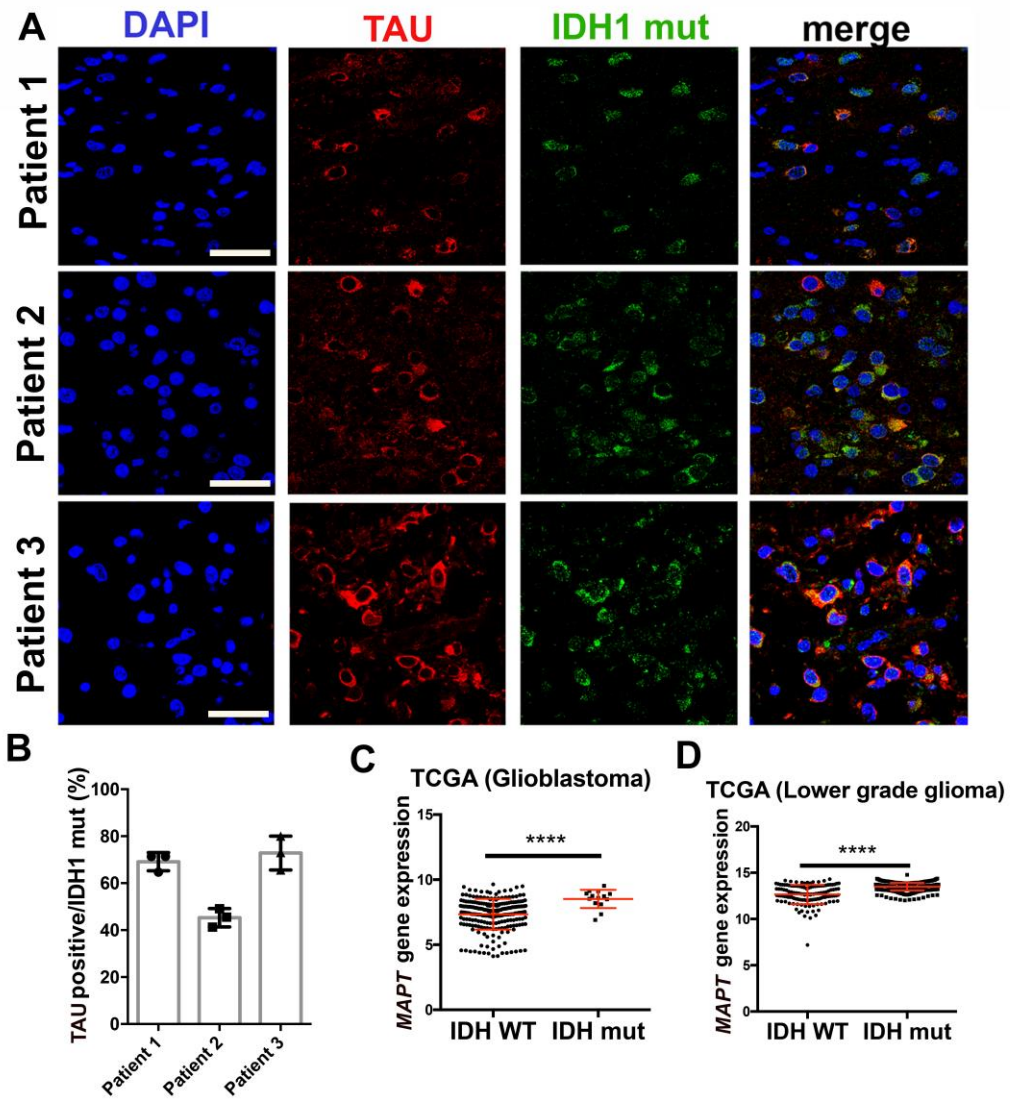

Fig. S3. TAU correlates with the presence of IDH mutations. (**A**) Representative images of TAU and IDH1 mut IF co-staining of tumors from three different patients. (**B**) Quantification of the co-staining of TAU and IDH1 mut in A (n=3). (**C** and **D**) Analysis of *MAPT* expression by RNAseq in the GBM (C) and the LGG (D) TCGA cohorts, grouped based on the presence of IDH mutations (n=692). Data shown as mean ± SD; Student's t test; ****, $p \leq 0.0001$. Scale bar 50 μm.

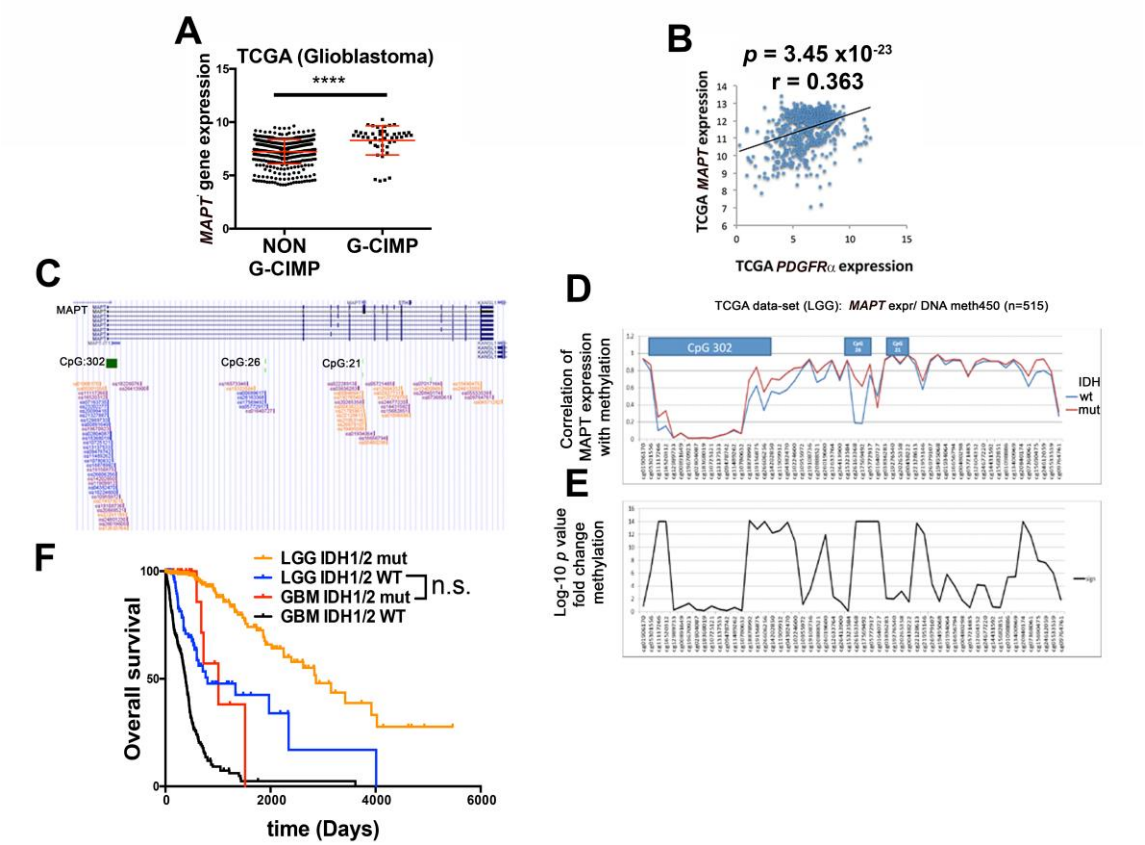

Fig. S4. The expression of *MAPT* is associated with the IDH mut DNA methylation phenotype. (**A**) Analysis of *MAPT* expression in GBM according to the level of CpG methylation: low-level methylator phenotype (NON G-CIMP) or high-level methylator phenotype (G-CIMP). (**B**) Correlation between the transcription of *MAPT and PDGFRA* (n=702) using the TCGA-merge (LGG+GBM) dataset and the Pearson's correlation test. (**C**) Organization of the possible CpG islets on the promoter zone of the *MAPT* gene using the methylation probes by genome browser. (**D** and **E**) Analysis of the fold change CpG methylation in 515 patients with LGG. The blue line shows the levels of methylation in gliomas with wt *IDH* and in red the level of methylation in gliomas with mutations in *IDH*. (**F**) Kaplan-Meier overall survival curves of LGG (n=451) and GBM (n=299) patients from the TCGA cohort, stratified based on the status of IDH1/2. Data shown as mean ± SD; Student's t test; ****, $p \leq 0.0001$; n.s., non-significant.

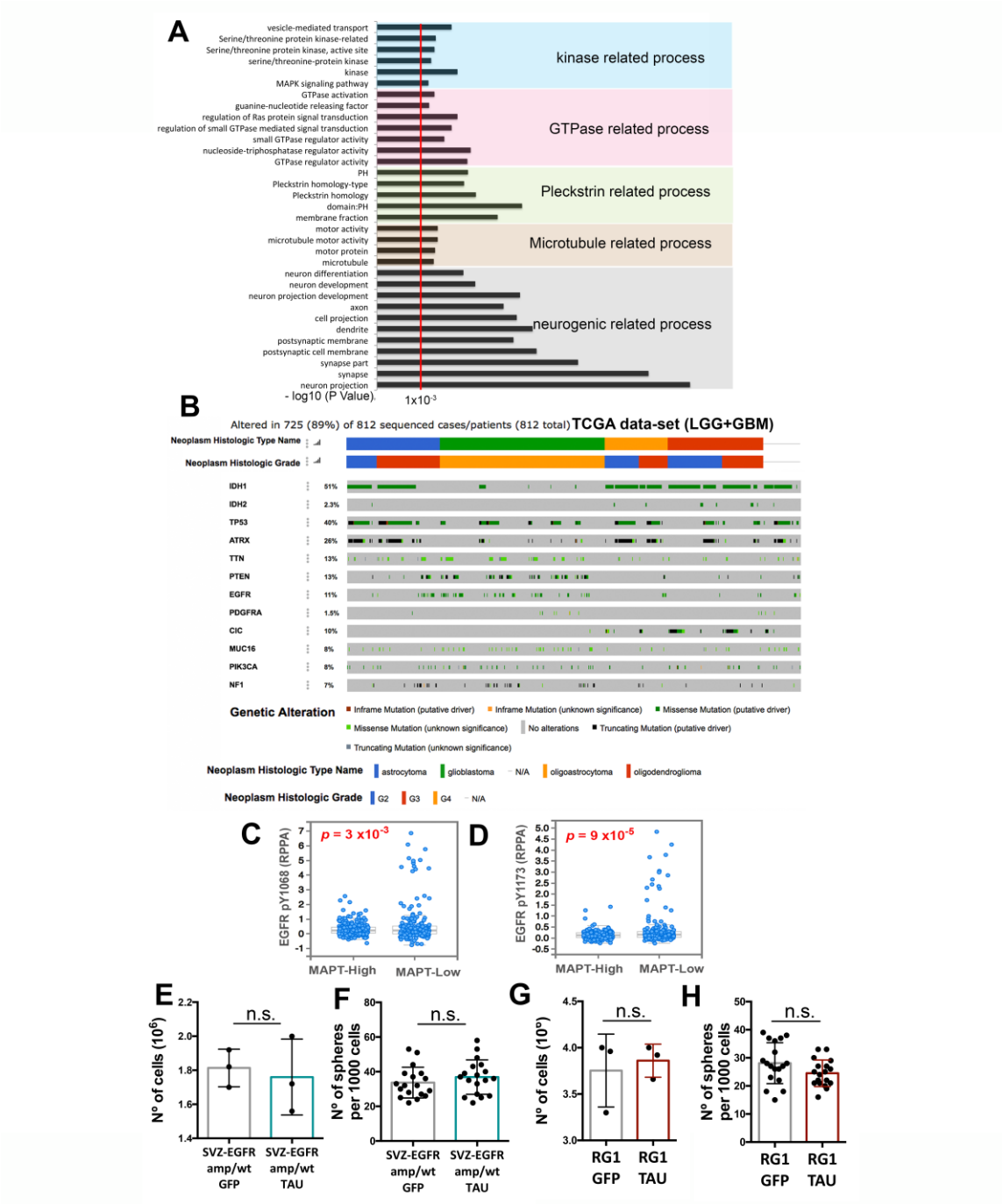

Fig. S5. Association of TAU function with the EGFR pathway in gliomas. (**A**) Top enriched Gene Ontology (GO) biological processes from the cluster of 500 genes that are co-expressed with *MAPT*. We used the LGG+GBM merge cohort and the DAVID gene ontology program. (**B**) Histogram showing the non-silent somatic mutations in genes commonly modified in diffuse gliomas grouped according to the WHO classification (histological type and grade). (**C and D**) Analysis of the amount of Phospho-Tyr1068-EGFR (C) and Phospho-Tyr1173-EGFR (D) in a cohort of 244 patients with GBM (TCGA-GBM dataset). Tumors were stratified into 2 groups based on high and low *MAPT* expression values. (**E** to **H**) Quantification of the number of cells

(**E** and **G**) and spheres (**F** and **H**) in SVZ-EGFRamp/wt (**E** and **F**) and RG1 (**G** and **H**) cells after the overexpression of GFP or TAU (n=3). Data shown as mean ± SD; Student's t test; n.s., non-significant.

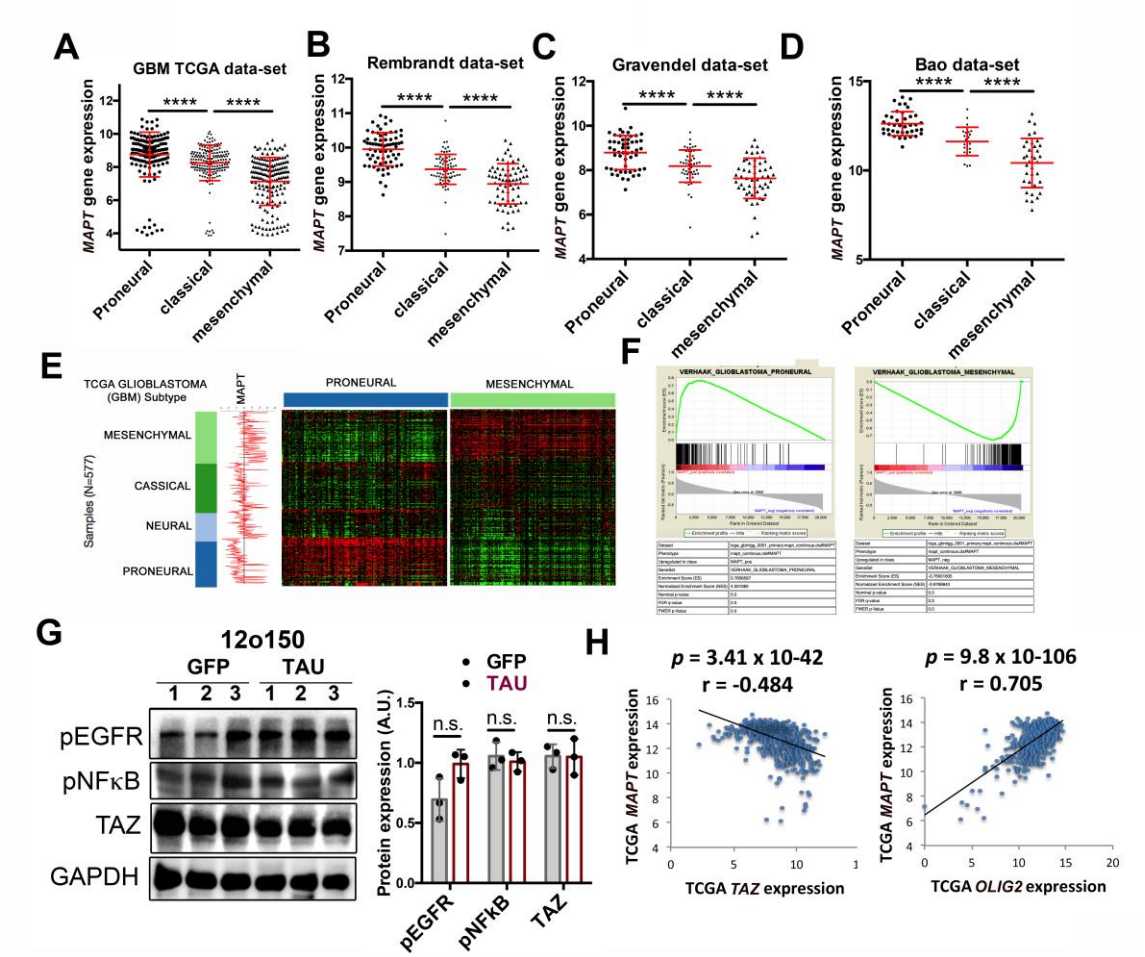

Fig. S6. Association of TAU with the different GBM subtypes and the NF-κB–TAZ axis. (**A** to **D**) Analysis of *MAPT* expression in the different GBM subtypes using the TCGA (n=528) (A), the Rembrandt (n=219) (B), the Gravendeel (n=159) (C) and the Bao (n=100) (D) data sets. (**E**) Analysis of the amount of *MAPT* mRNA in the different GBM subtypes (left) and heatmap of PN and MES gene expression signature depending on the transcription of *MAPT* (right). (**F**) GSEA enrichment plot analysis using *MAPT* gene expression values as template and PN or MES signatures. (**G**) WB analysis of phospho-EGFR, phosphor-NF-κB and TAZ in 12o150 xenografts expressing either GFP or TAU. GADPH levels were used for normalization (n=3). Quantification is shown on the right. (**H**) Scatter plots showing the correlation between the expression of *MAPT* and *TAZ* (left) or between *MAPT* and *OLIG2* (right) across 703 glioma samples. Pearson's correlation test was used. Data shown as mean ± SD; Student's t test; ****, $p \leq 0.0001$; n.s., non-significant.

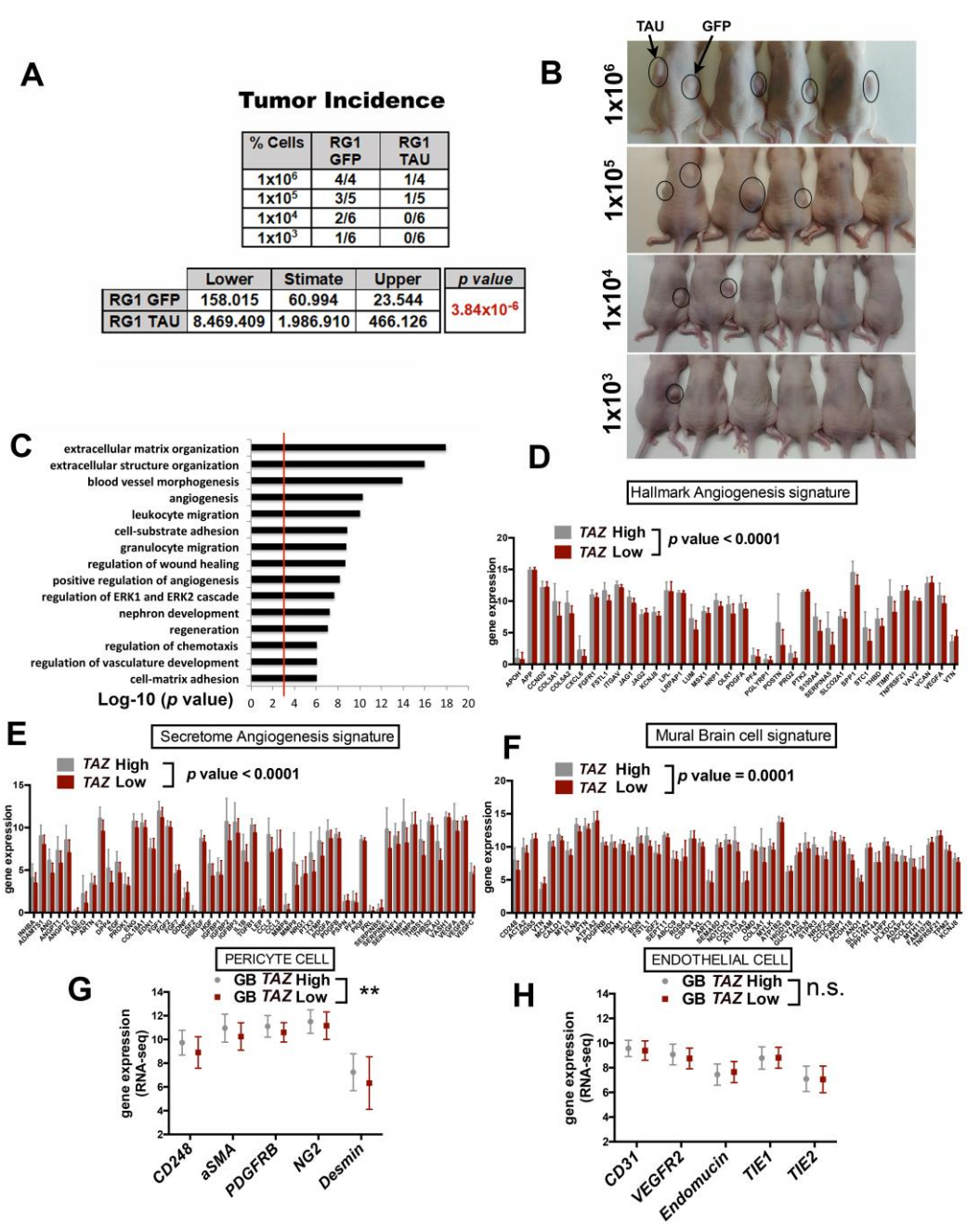

Fig. S7. Vascular phenotypes associated with TAZ in gliomas. (**A** and **B**) Subcutaneous tumor growth assay (limited dilution) of RG1 cells after overexpression of GFP or TAU (n=4 to 6). The statistical analysis is shown on the bottom and the image of the animals before tumor dissection is shown in B. (**C**) The top 15 gene ontology (GO) terms associated with cluster from the 500 genes that correlate positively with the expression of *TAZ* in TCGA-LGG+GBM dataset. GO terms were ranked by p value. (**D** to **F**) Angiogenesis (**D**), angiogenic secretome (**E**) and mural brain cell (**F**) signatures in gliomas of the TCGA-LGG+GBM-merge data-set. Tumors were classified as High or Low *TAZ*-expressing gliomas (n=702). (**G** and **H**) Analysis of the expression (RNAseq)

of the 5 most significant genes associated with pericytes (G) or endothelial cells (H); signature including the most relevant genes for biological processes associated with vasculogenesis, angiogenesis and secretion in (C-F). Data shown as mean ± SD; Paired t test; ** $p \leq 0.01$, n.s. non significant.

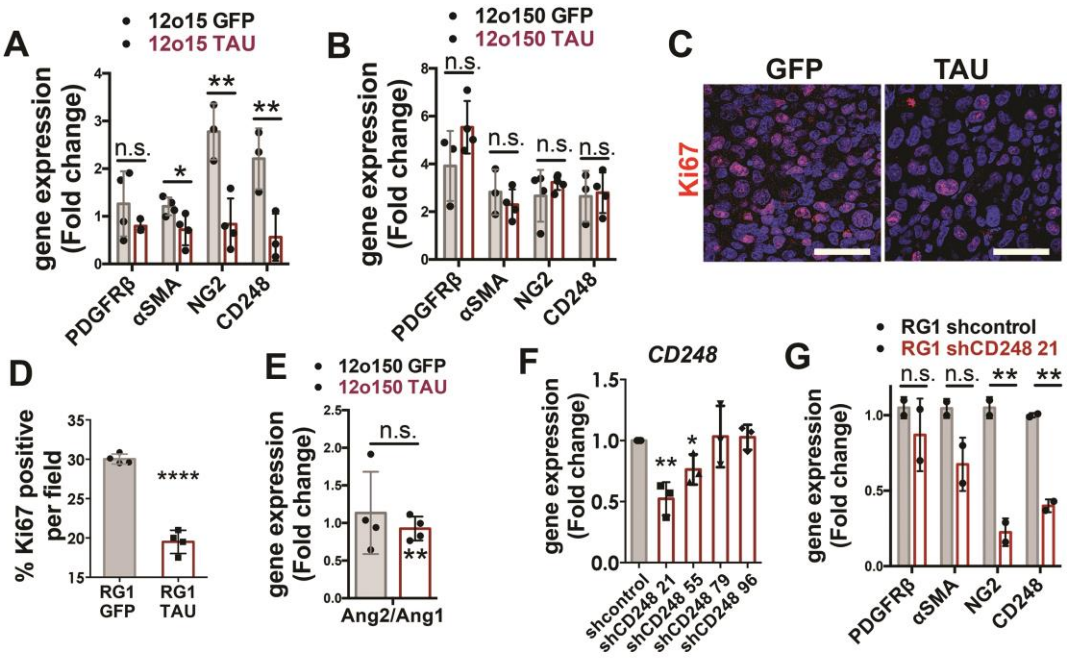

Fig. S8. Implication of the tumor-derived pericytes on the glioma vasculature and growth. (**A** and **B**) qRT-PCR analysis of pericytic–related genes (using human-specific primers) in 12o15 (A) and 12o150 (B) xenografts expressing GFP or TAU (n=3 to 4). Mouse cDNA was used as a negative control. The expression of *HPRT* was used for normalization**.** (**C** and **D**) Representative images of Ki67 IF staining of sections from RG1 xenografts expressing GFP or TAU (C) and quantification of the number of Ki67 positive cells per field (D) (n=4). (**E**) Ratio of *Ang2/Ang1* expression measured by qRT-PCR in 12o150 tumors. The expression of *HPRT* was used for normalization (n=4). (**F**) qRT-PCR analysis of *CD248* mRNA after transduction of different shRNAs against the *CD248* gene in RG1 cells (n=3). The expression of *HPRT* was used for normalization. (**G**) qRT-PCR quantification of 4 pericyte markers: *CD248, NG2, αSMA* and *PDGFRβ*, after the transduction of shcontrol or shCD248 21 in the RG1 line (n=3). The expression of *HPRT* was used for normalization. Data shown as mean ± SD; Student's t test; *, $p \leq 0.05$; **, $p \leq 0.01$; ****, $p \leq 0.0001$, n.s., non-significant. Scale bar 50 μm.

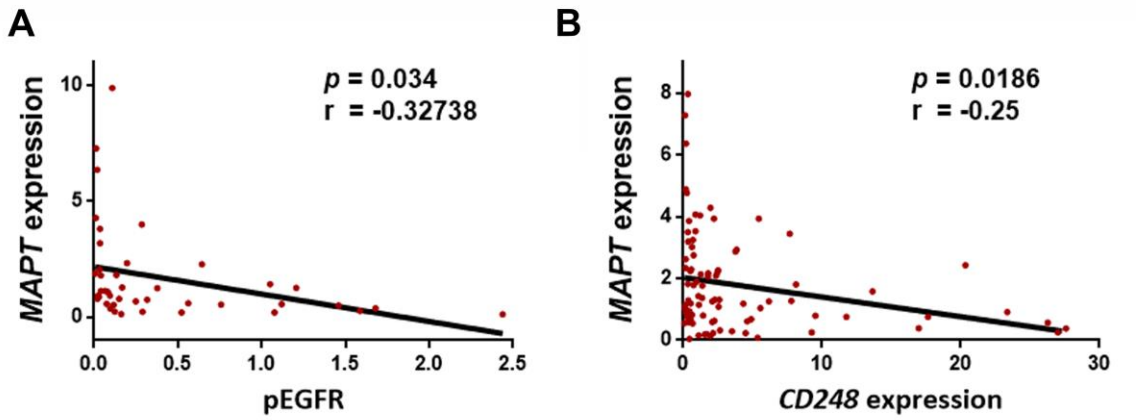

Fig. S9 TAU negatively correlates with EGFR signaling and *CD248* expression. Scatter plots showing the correlation between the expression of *MAPT* and the amount of pEGFR (n=42) (A) or between *MAPT* and *CD248 transcription (n=88)* (B) in our own glioma samples cohort. Pearson's correlation test was used.

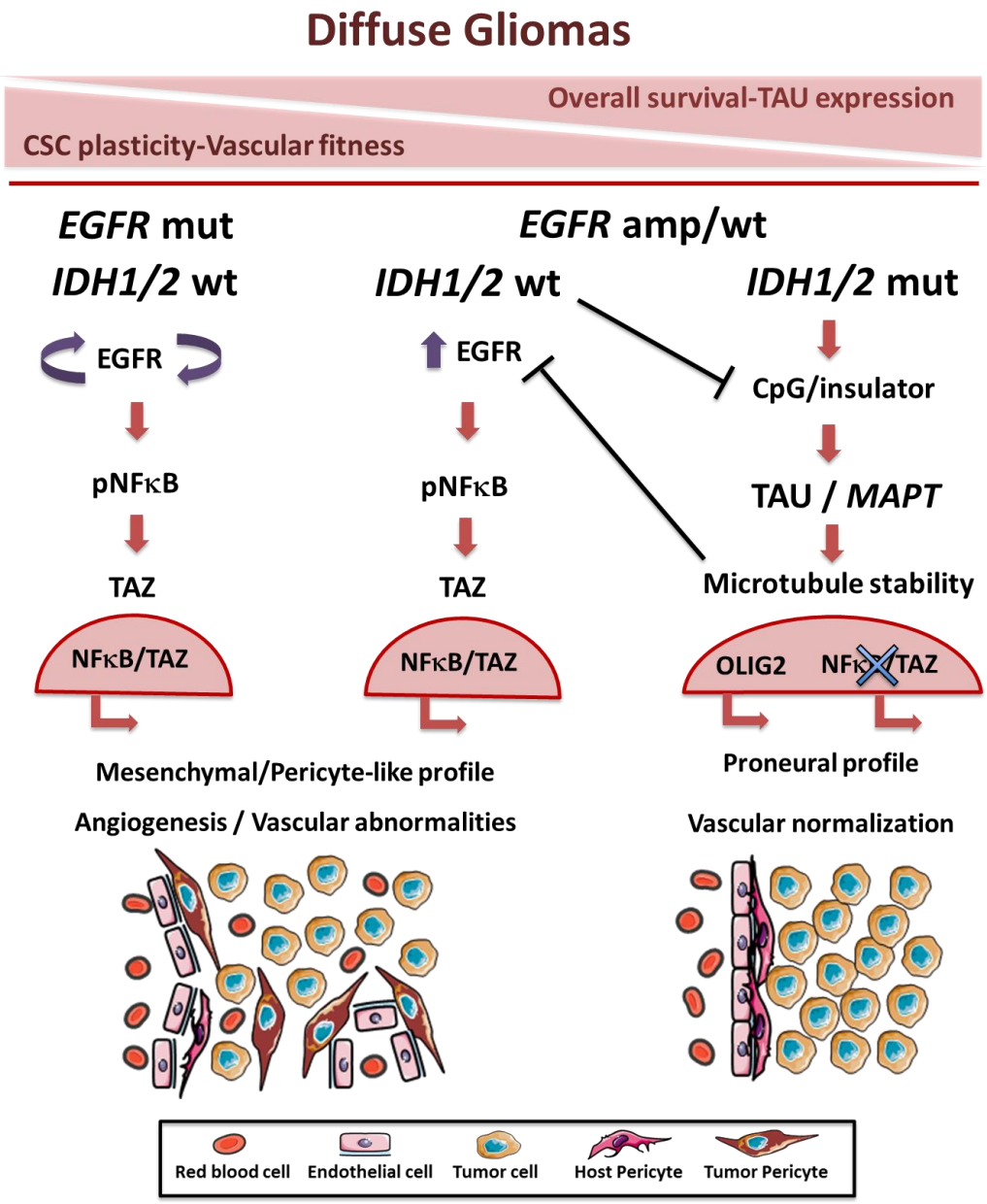

Fig. S10. The vascular phenotype of gliomas is determined by the genetic status of *EGFR* and *IDH* and by the expression of TAU. EGFRmut and EGFRamp glioma cells have the capacity to transdifferentiate into mesenchymal/pericyte-like cells. These tumor pericytes are master regulators of the angiogenic processes, shaping the vascular phenotype and the proliferative capacity of the tumors. In IDH mut tumors, TAU expression is epigenetically induced and impairs the appearance of tumor pericytes by inhibiting the EGFR-NF-*K*B-TAZ axis. As a consequence, TAU promotes the normalization of the vasculature and the appearance of a Proneural profile, but only in the absence of mutations in *EGFR*

Table S1. Human samples.

Sample	Hospital	Diagnosis	Grade	Tau IHC	IDH	ATRX
1	H12O	Glioblastoma	IV	0	wt	wt
2	H12O	Glioblastoma	IV	0	wt	wt
3	H12O	Glioblastoma	IV	1	wt	wt
4	H12O	Glioblastoma	IV	0	wt	wt
5	H12O	Glioblastoma	IV	0	wt	wt
6	H12O	Glioblastoma	IV	2	wt	wt
7	H12O	Glioblastoma	IV	3	wt	wt
8	H12O	Glioblastoma	IV	3	wt	wt
9	H12O	Glioblastoma	IV	1	wt	wt
10	H12O	Glioblastoma	IV	1	wt	wt
11	H12O	Glioblastoma	IV	0	wt	wt
12	H12O	Anaplastic Astrocytoma	nd	3	mut	wt
13	H12O	Glioblastoma	IV	1	wt	wt
14	H12O	Glioblastoma	IV	0	wt	mut
15	H12O	Glioblastoma	IV	1	wt	mut
16	H12O	Glioblastoma	IV	2	wt	wt
17	H12O	Glioblastoma	IV	3	wt	wt
18	H12O	Glioblastoma	IV	2	wt	mut
19	H12O	Glioblastoma	IV	0	wt	wt
20	H12O	Glioblastoma	IV	0	wt	wt
21	H12O	Glioblastoma	IV	1	wt	wt
22	H12O	Glioblastoma	IV	0	wt	wt
23	H12O	Glioblastoma	IV	1	wt	wt
24	H12O	Glioblastoma	IV	0	wt	wt
25	H12O	Glioblastoma	IV	1	wt	mut
26	H12O	Glioblastoma	IV	3	wt	wt
27	H12O	Glioblastoma	IV	1	wt	wt
28	H12O	Glioblastoma	IV	0	wt	wt
29	H12O	Glioblastoma	IV	0	wt	wt
30	H12O	Glioblastoma	IV	1	wt	wt
31	H12O	Glioblastoma	IV	1	wt	wt
32	H12O	Glioblastoma	IV	0	wt	wt
33	H12O	Glioblastoma	IV	0	wt	wt
34	H12O	Oligodendroglioma	nd	1	mut	wt
35	H12O	Oligodendroglioma	III	2	mut	wt
36	H12O	Diffuse mindline glioma	nd	2	wt	mut
37	H12O	Anaplastic Astrocytoma	III	0	wt	wt
38	H12O	Astrocytoma	II	1	wt	nd
39	H12O	Anaplastic Astrocytoma	III	3	mut	mut
40	H12O	Anaplastic Astrocytoma	III	3	mut	mut
41	H12O	Diffuse Astrocytoma	II	3	mut	mut

42	H12O	Anaplastic Astrocytoma	III	3	wt	mut
43	H12O	Diffuse Astrocytoma	II	3	wt	wt
44	H12O	Anaplastic Astrocytoma	III	1	mut	mut
45	H12O	Anaplastic Astrocytoma	III	2	mut	nd
46	H12O	Anaplastic Astrocytoma	III	3	wt	wt
47	H12O	Anaplastic Astrocytoma	III	2	mut	mut
48	H12O	Anaplastic Astrocytoma	III	3	wt	wt
49	H12O	Anaplastic Astrocytoma	III	0	mut	nd
50	H12O	Astrocytoma	II	2	mut	nd
51	H12O	Anaplastic Astrocytoma	III	3	wt	mut
52	H12O	Glioblastoma	IV	3	mut	mut
53	H12O	Astrocytoma	II	2	mut	mut
54	H12O	Anaplastic Astrocytoma	III	3	mut	mut
55	H12O	Anaplastic Astrocytoma	III	1	wt	wt
56	H12O	Anaplastic Astrocytoma	III	0	mut	mut
57	H12O	Anaplastic Astrocytoma	III	3	mut	mut
58	H12O	Anaplastic Astrocytoma	III	3	mut	nd
59	H12O	Anaplastic Astrocytoma	III	3	mut	nd
60	H12O	Anaplastic Astrocytoma	III	1	mut	mut
61	H12O	Anaplastic Astrocytoma	III	2	mut	mut
62	H12O	Astrocytoma	II	3	mut	mut
63	H12O	Diffuse Astrocytoma	II	2	mut	mut
64	H12O	Anaplastic Astrocytoma	III	3	mut	mut
65	H12O	Astrocytoma	II	2	wt	nd
66	H12O	Diffuse Astrocytoma	II	3	mut	mut
67	H12O	Anaplastic Astrocytoma	III	1	mut	mut
68	H12O	Anaplastic Astrocytoma	III	1	wt	nd
69	H12O	Anaplastic Astrocytoma	III	3	wt	nd
70	La Fe	Glioblastoma	IV	0	nd	nd
71	La Fe	Glioblastoma	IV	0	nd	nd
72	La Fe	Glioblastoma	IV	0	nd	nd
73	La Fe	Glioblastoma	IV	0	nd	nd
74	La Fe	Glioblastoma	IV	0	nd	nd
75	La Fe	Glioblastoma	IV	0	nd	nd
76	La Fe	Glioblastoma	IV	0	nd	nd
77	La Fe	Glioblastoma	IV	0	nd	nd
78	La Fe	Glioblastoma	IV	0	nd	nd
79	La Fe	Glioblastoma	IV	0	nd	nd

80	La Fe	Glioblastoma	IV	0	nd	nd
81	La Fe	Oligodendroglioma	nd	1	nd	nd
82	La Fe	Glioblastoma	IV	2	nd	nd
83	HGM	Glioblastoma	IV	1	nd	nd
84	HGM	Oligoastrocytoma	II	2	mut	nd
85	HGM	Oligodendroglioma	II	3	mut	nd
86	La Fe	Glioblastoma	IV	0	nd	nd
87	La Fe	Glioblastoma	IV	2	nd	nd
88	La Fe	Glioblastoma	IV	1	nd	nd
89	La Fe	Glioblastoma	IV	0	nd	nd
90	La Fe	Glioblastoma	IV	0	nd	nd
91	La Fe	Glioblastoma	IV	0	nd	nd
92	La Fe	Anaplastic Oligoastrocytoma	III	2	nd	nd
93	La Fe	Anaplastic Oligoastrocytoma	III	3	mut	nd
94	La Fe	Diffuse Glioma	II	3	mut	nd
95	La Fe	Glioblastoma	IV	2	wt	nd
96	La Fe	Glioblastoma	IV	0	wt	nd
97	La Fe	Glioma difuso anaplásico, de fenotipo astrocitario	III	2	mut	nd
98	La Fe	Glioma difuso anaplásico, de fenotipo astrocitario	III	2	mut	mut
99	La Fe	Glioblastoma	IV	2	wt	nd
100	La Fe	Glioma difuso de fenotipo oligodendroglial	II	1	mut	wt
101	La Fe	Oligodendroglioma	II	1	mut	wt
102	La Fe	Glioblastoma	IV	2	wt	wt

Table S2. Paired human samples.

Sample	Hospital	Year of surgery	Progression Free Survival	Diagnosis	Grade	Tau IHC	IDH	ATRX
3	H12O	2010		Astrocytoma	III	2.6	mut	mut
	H12O	2011	18 months	Astrocytoma	III	1.6	mut	mut
5	H12O	2009		Astrocytoma	II	2.3	mut	mut
	H12O	2011	22 months	Glioblastoma	IV	0.7	mut	mut
6	H12O	2008		Oligodendroglioma	III	1.6	mut	wt
	H12O	2011	29 months	Oligodendroglioma	III	1.5	mut	wt
7	H12O	2014		Astrocytoma	II	1.2	mut	mut
	H12O	2016	19 months	Glioblastoma	IV	0.2	mut	mut
8	H12O	2013		Astrocytoma	II	1.7	mut	mut
	H12O	2018	50 months	Astrocytoma	III	0.8	mut	mut
10	H12O	2010		Astrocytoma	II	1.2	mut	mut
	H12O	2018	100 months	Astrocytoma	II	1.7	mut	mut
11	H12O	2012		Astrocytoma	III	1.2	mut	mut
	H12O	2015	39 months	Glioblastoma	IV	0.0	mut	mut
13	H12O	2013		Astrocytoma	II	1.5	mut	mut
	H12O	2016	42 months	Astrocytoma	II	2.6	mut	mut

Table S3. GBM cell lines. (nd: not diagnosed. 0: wild type. 1: altered)

Cell line	Origin	EGFR amp	EGFR mut	PTEN loss	p53 mutation
RG1	Mazzoleni et al.	1	0	0	1
12o01	Hospital 12 de Octubre	1	1 (vIII)	0	1
12o02	Hospital 12 de Octubre	0	0	1	1
12o12	Hospital 12 de Octubre	1	1(vIII)	nd	0
12o15	Hospital 12 de Octubre	0	0	0	1
12o16	Hospital 12 de Octubre	0	mut	nd	nd
12o22	Hospital 12 de Octubre	1	1(vIII)	nd	nd
12o29	Hospital 12 de Octubre	nd	nd	nd	nd
12o33	Hospital 12 de octubre	1	nd	nd	nd
12o40	Hospital 12 de octubre	nd	nd	nd	nd
12o43	Hospital 12 de Octubre	nd	nd	nd	nd
12o44	Hospital 12 de Octubre	nd	nd	nd	nd
12o49	Hospital 12 de Octubre	1	1 (vII)	nd	nd
12o53	Hospital 12 de Octubre	nd	nd	nd	nd
12o56	Hospital 12 de Octubre	nd	nd	nd	nd
12o84	Hospital 12 de Octubre	1	1 C.1118C>A	0	0
12o89	Hospital 12 de Octubre	0	1 V774M	mut	1
12o107	Hospital 12 de Octubre	0	0	0	1
12o108	Hospital 12 de Octubre	0	0	0	0
12o113	Hospital 12 de Octubre	1	0	0	0
12o116	Hospital 12 de Octubre	nd	nd	nd	Nd
12o121	Hospital 12 de Octubre	1	0	1	0
12o124	Hospital 12 de Octubre	1	nd	nd	nd
12o126	Hospital 12 de Octubre	0 1	1 G1134S	1	1
12o129	Hospital 12 de Octubre	Nd	nd	nd	nd
12o150	Hospital 12 de Octubre	0	1 L760P/M945I	mut	1
GB4	Hospital Ramón y Cajal	nd	nd	Nd	1
GB19	Hospital Ramón y Cajal	nd	nd	nd	1

Table S4. Antibodies.

Antibody	Dilution	Source
Acetyl-Tubulin	1:5000 (WB)	Sigma
AKT	1:1000 (WB)	Cell Signaling (4691)
ANGPT2	1:100(IF)	Santa Cruz Biotechnology (SC-74403)
α SMA	1:500 (WB) 1:100 (IHC)	Santa Cruz Biotechnology (SC-32251)
β-Actin	1:1000 (WB)	Sigma
β-catenin	1:1000 (WB)	Cell
BrdU	1:100 (IHC)	Dako
CD248	1:500 (WB)	Santa Cruz Biotechnology (SC-377221)
EGFR	1:1000 (WB)	Cell Signaling (2232)
Endomucin	1:100 (IF)	Santa Cruz Biotechnology (SC-65495)
GAPDH	1:500 (WB)	Santa Cruz Biotechnology (SC-47724)
GFP	1:100(IHC)	Santa Cruz Biotechnology
NG2		
OLIG2	1:100(IHC)	Santa Cruz Biotechnology
phospho-Ser431 AKT	1:1000 (WB)	Cell Signaling (4549)
phospho-Tyr751 PDGFRB	1:1000 (WB)	Cell Signaling (4549)
phospho-Tyr740 PDGFRB	1:100 (IHC)	SIGMA (SAB4504202)
PDGFRB	1:1000 (WB)	Cell Signaling (4564)
phospo-Tyr1068 EGFR	1:1000 (WB)	Cell Signailing (3777)
phospo-Ser536 NFK β	1:1000 (WB)	Cell Signaling (3033)
TAU 7.51	1:500 (WB)	
TAU-5	1:500	Calbiochem (577801)
TAU-12	1:500	Millipore (MAB2241)
TAU	(IHQ)	Dako
YAP-TAZ	1:1000 (WB) 1:50 (IHC)	Cell Signaling SIGMA

anti mouse -Dylight 488	1:500 (IF)	Jackon Immunoresearch
anti rabbit -Dylight 488	1:500 (IF)	Jackon Immunoresearch
Anti mouse-Cy3	1:500 (IF)	Jackon Immunoresearch
Anti rabbit-Cy3	1:500 (IF)	Jackon Immunoresearch
Anti rat-Cy5	1:500 (IF)	Jackon Immunoresearch

Table S5. qRT-PCR primers.

Specie	gene	Forward (5'-3´)	Reverse (3'-5´)
mouse	CD31	TCCAGGTGTGCGAAATGCT	TGGCAGCTGATGCCTATGG
mouse	ENG	TGCACTTGGCCTACGACTC	TGGAGGTAAGGGATGGTAGCA
mouse	VE-CAD	TTACTCAATCCACATACACATTTTCG	GCATGATGCTGTACTTGGTCATC
mouse	CD248	TTGATGGCACCTGGACAGAGGA	TCCAGGTGCAATCTCTGAGGCT
mouse	αSMA	ACCATCGGCAATGAGCGTTTCC	GCTGTTGTAGGTGGTCTCATGG
mouse	PDGFRB	CCGGAACAAACACACCTTCT	TATCCATGTAGCCACCGTCA
mouse	MMP9	GCAAGGGGCCGTGTCTGGAGATTC	GCCCACGTCGTCCACCTGGTT
mouse	LMNA	TTGCCTCAACTGCAATGACAA	TCTCGATGTCGGTAAAACCCC
mouse	KDR	TTTGGCAAATACAACCCTTCAGA	GCAGAAGATACTGTCACCACC
mouse	VEGFR2	CATCACCGAGAACAAGAACAAAACT	GATACCTAGCGCAAAGAGACACATT
mouse	TEK	ACGGACCATGAAGATGCGTCAACA	TCACATCTCCGAACAATCAGCCTGG
mouse	NRP1	GCTTGTGCTCTATGCAGATCG	TCGACGAACTCCTGGTGATTTA
mouse	EPHA2	GCACAGGGAAAGGAAGTTGTT	CATGTAGATAGGCATGTCGTCC
mouse	AQP1	AGGCTTCAATTACCCACTGGA	GTGAGCACCGCTGATGTGA
mouse	VEGF A	TGCCAAGTGGTCCCAGGCTGC	CCTGCACAGCGCATCAGCGG
mouse	PDGF A	GATACCTCGCCCATGTTCTG	CAGGCTGGTGTCCAAAGAAT
mouse	PDGF B	GGGCCCGGAGTCGGCATGAA	AGCTCAGCCCCATCTTCATCTTACGG
mouse	PGF	GAGGCCAGAAAGTCAGGGGGC	ATGGGCCGACAGTAGCTGCGA
mouse	CCL2	AGGTCCCCTGTCATGCTTCTG	TCTCCAGCCTACTCATTGGG
mouse	PI3KCG	GCTCTTCGCCAATCACACAAAC	GGCATTCCTGTCATCAGCATC
mouse	NG2	GACGGCGCACACACTTCTC	TGTTGTGATGGGCTTGTCAT
mouse	Ang1	CATTCTTCGCTGCCATTCTG	GCACATTGCCCATGTTGAATC
mouse	Ang2	TTAGCACAAAGGATTCGGACAAT	TTTTGTGGGTAGTACTGTCCATTCA
human	MAPT	GTCGAAGATTGGGTCCCTGG	GACACCACTGGCGACTTGTA
human	αSMA	TAGCACCCAGCACCATGAAGATCA	GAAGCATTTGCGGTGGACAATGGA
human	NG2	AGCTCTACTCTGGACGCC	ATCGACTGACAACGTGGC
human	CD248	AGACCACCACTCATTTGCCTGGAA	AGTTGGGATAATGGGAAGCGTGGT
human	PDGFRB	ACGGCTCTACATCTTTGTGCCAGA	TCGGCATGGAATGGTGATCTCAGT
human	SNAIL 1	ACCACTATGCCGCGCTCTT	GGTCGTAGGGCTGCTGGAA
human	SNAIL 2	ATCTGCGGCAAGGCGTTTTCCA	GAGCCCTCAGATTTGACCTGTC
human	ZEB 1	GGCATACACCTACTCAATACGG	TGGGCGGTGTAGAATCAGAGTC
human	ZEB 2	AATGCACAGAGTGTGGCAAGGC	CTGCTGATGTGCGAACTGTAGC
human	TWIST 1	CCGGAGACCTAGATGTCATTG	CACGCCCTGTTTCTTTGAAT
human	SERPINE	CATAGTGGAAGTGATAGAT	ACTCTGTTAATTCGTCTT
human	TAZ	TTTCCTCAATGGAGGGCCA	GGGTGTTTGTCCTGCGTTTT
human	CD133	GCCACCGCTCTAGATACTGC	TGTTGTGATGGGCTTGTCAT
human	SOX2	GCGAACCATCTCTGTGGTC	AATGGAAAGTTGGGATCGAA
human	L1 CAM	TCGCCCTATGTCCACTACACCT	ATCCACAGGGTTCTTCTCTGGG
human	DLL3	AAACCTATGGGCTTGAGGAG	CGCTGAGTACAATCAGTGGAA
human	REST	CGGCTAACAATACTAATCG	TAGACTCGCTCATTATCC
human	LIF	CATGAACCAGATCAGGAG	GCTGTGTAATAGAGAATAAAGAG
human	NESTIN	GCGGCTGCGGGCTACTGAAA	CCAGCTGCTGCCGACCTTCC
human	OLIG2	CGGCTTTCCTCTATTTTGGTT	GTTACACGGCAGACGCTACA

Table S6. Sequencing primers.

Species	Gene name	Forward (5'-3´)	Reverse (3'-5´)
human	**EGFR**	CAGTATTGATCGGGAGAG	CATCTCATAGCTGTCGGC
		CAACATGTCGATGGACTTCCA	TTCGCATGAAGAGGCCGATC
		GCCCCCACTGCGTCAAGACC	AGCTTTGCAGCCCATTTCTA-
		CAGCGCTACCTTGTCATTCA	CTATCCTCCGTGGTCATGCT

Data file S1. Raw data. Provided as a separate Excel file.